

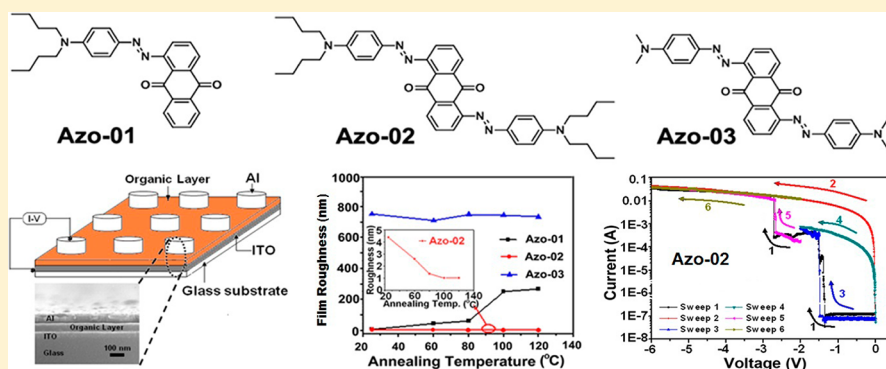
# Thermally Stable Ternary Data-Storage Device Based on Twisted Anthraquinone Molecular Design

Yuhui Zhang,<sup>†</sup> Hao Zhuang,<sup>†</sup> Yong Yang,<sup>†</sup> Xufeng Xu,<sup>†</sup> Qing Bao,<sup>†</sup> Najun Li,<sup>†</sup> Hua Li,<sup>\*,†</sup> Qingfeng Xu,<sup>†</sup> Jianmei Lu,<sup>\*,†,‡</sup> and Lihua Wang<sup>†</sup>

<sup>†</sup>Key Laboratory of Organic Synthesis of Jiangsu Province, College of Chemistry, Chemical Engineering and Materials Science, Soochow University, 199 Ren'ai Road, Suzhou 215123, China

<sup>‡</sup>Institute of Chemical Power Sources, Soochow University, Suzhou, Jiangsu 215006, China

## Supporting Information



**ABSTRACT:** Three donor–acceptor and twisted anthraquinone azo molecules were synthesized, and the effects of conjugated backbone length, alkyl chains length, and the thermal annealing temperature on the memory characteristics were explored. The device based on Azo-02, which has longer conjugated backbone and alkyl chains, exhibited stable nonvolatile ternary memory behavior as the thermal annealing temperature increased, with basically the same switching threshold voltages and current ratios being  $\sim 1:10^{3.43}:10^{5.50}$ . For the “counterpart” molecules (Azo-01 and Azo-03) film, defects appeared or disordered, crystal packing formed as the thermal annealing temperature increased, and the corresponding devices exhibited no obvious conductance switching behaviors. The mechanism related to electrical switching properties and WORM (write-once-read-many-times) behaviors were elucidated through molecular simulation. The results demonstrated that the long-term thermally stable high-density data-storage devices can be fabricated by adjusting the structures of twisted molecules.

## 1. INTRODUCTION

Organic/polymer memories are considered to be an alternative or supplementary technology to the conventional data-storage devices due to their low-cost, structural flexibility, and three-dimensional stacking capability.<sup>1–7</sup> In recent years, numerous memory devices based on electroactive organic/polymer materials have been reported.<sup>8–12</sup> However, they are limited to electrical bistability (i.e., “0” and “1”).<sup>13</sup> Recently, the organic and polymer materials with three distinct conductivity states under an external electric field corresponding to ternary data-storage utilities have been reported.<sup>13–15</sup> As compared to the traditional binary system, ternary data-storage devices can store more than 2-bits in a single cell; thus the storage density of the devices was increased exponentially. Such devices have been less-explored, partly because of the lack of appropriate materials.

The long-term stable electrical devices have been recognized as an important area of research.<sup>16,17</sup> It is found that many factors of electroactive organic/polymer layer, including surface roughness, continuity, thickness, and agglomerated morphol-

ogy, have significant effects on the performance of the devices.<sup>18–21</sup> Therefore, to achieve one stable ternary data-storage device, reducing the temperature fluctuation of the electroactive organic/polymer layer is an effective method. Several studies on the thermal stability of polymer film have been studied, including doping,<sup>16</sup> thermal cross-linking,<sup>22</sup> and photo cross-linking technologies.<sup>23–24</sup> Similar work has also been investigated in organic field-effect transistors and solar cells for small molecules, which are limited to planar molecules and approximately planar molecules.<sup>25–27</sup> These molecules easily form crystalline films by intermolecular  $\pi$ – $\pi$  stacking interactions under high thermal annealing temperature. Our group has found that the  $\pi$  conjugated length played an important role in the device performance,<sup>28</sup> as the double length molecule showed stable film quality from 25 to 100 °C; however, when the temperature is over 100 °C, the film’s

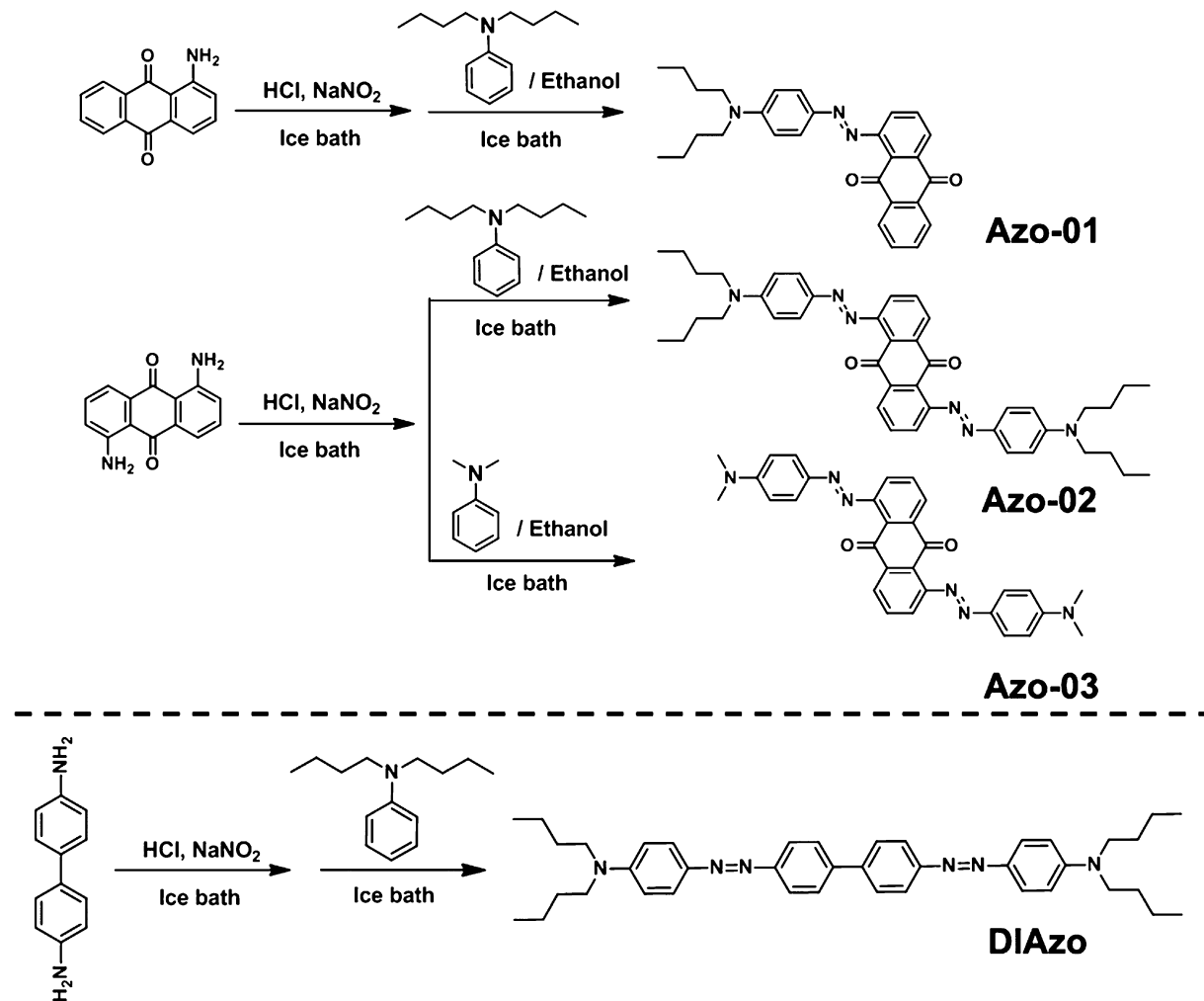
Received: June 6, 2012

Revised: September 24, 2012

Published: October 8, 2012



Scheme 1. Chemical Structures and Synthesis Routes of Four Small Molecules



surface appeared to have obvious holes. Azobenzene derivatives have been widely used for optoelectronic data storage because of their long-term charge trapping and storing properties and good structure expandability.<sup>10a,18a,29–31</sup> In this work, we report series of donor–acceptor conjugated twisted anthraquinone-azo molecules (Scheme 1). The different conjugated length and different alkyl chains were designed into the molecules to improve the device's performance. The electroactive layers vacuum deposited by **Azo-02**, which contained the double conjugated backbone and longer alkyl chains, could retain invariable film quality from room temperature to 125 °C, and the corresponding devices show excellent ternary data-storage performance, while the “counterpart” molecules, **Azo-01** and **Azo-03**, exhibit poor film stability and even have no typical electrical characteristics. The result shows that suitable length of the conjugated backbone and alkyl chain could lead to a well  $\pi$ – $\pi$  stacked film.

## 2. EXPERIMENTAL SECTION

**2.1. Materials.** 1-Aminoanthraquinone (99%), 1,5-diamineanthraquinone (99%), benzidine (99%), and *N,N*-dibutylaniline (99%) were purchased from TCI chemical Reagent Co. Ltd., Japan. Sodium nitrite (99%), sodium hydroxide (99%), *N,N*-dimethylaniline (99%), and all solvents were purchased from Sinopharm Chemical Reagent Co. Ltd., China. All materials were used as received.

**2.2. Preparation of Molecules.** The compounds were prepared as detailed in Scheme 1.

**Synthesis of 1-((4-(Dibutylamino)phenyl)diazényl)-anthracene-9,10-dione (Azo-01).** A solution of sodium nitrite (0.68 g, 10 mmol) in water (5 mL) was added dropwise to the mixture of 1-aminoanthraquinone (2.32 g, 10 mmol), concentrated hydrochloric acid (8 mL), and water (25 mL) during 1 h at 0–2 °C. The mixture was stirred at 0–2 °C for 45 min. Next, the diazonium salt solution was added slowly to the solution of *N,N*-dibutylaniline (4.39 g, 10 mmol) in ethanol (80 mL) at 0–5 °C. The resultant colored mixture was stirred at 0–5 °C for 4 h. The solution was filtered, and the filtrate was dried in vacuum and purified by silica gel chromatography. Yield: 44.70%. <sup>1</sup>H NMR (400 MHz, CDCl<sub>3</sub>) δ (ppm): 8.23–8.33 (m, 3H), 7.94 (d, *J* = 9.1 Hz, 2H), 7.83–7.73 (m, 3H), 7.55 (d, *J* = 7.1 Hz, 1H), 6.73 (d, *J* = 9.1 Hz, 2H), 3.39 (t, *J* = 7.1 Hz, 4H), 1.70–1.55 (m, 4H), 1.37–1.43 (m, 4H), 0.99 (t, *J* = 7.3 Hz, 6H). HRMS: calcd for C<sub>28</sub>H<sub>29</sub>N<sub>3</sub>O<sub>2</sub> [M + H]<sup>+</sup> 440.2260, found 440.2333.

**Synthesis of 1,5-Bis((4-(dibutylamino)phenyl)diazényl)-anthracene-9,10-dione (Azo-02).** The compound was prepared by treatment of 1,5-diamineanthraquinone (2.48 g, 10 mmol) with *N,N*-dibutylaniline (4.10 g, 20 mmol) as described for **Azo-01**. Yield: 87.50%. <sup>1</sup>H NMR (300 MHz, CDCl<sub>3</sub>) δ (ppm): 8.27 (d, *J* = 7.2 Hz, 2H), 7.95 (d, *J* = 8.6 Hz, 4H), 7.77 (t, *J* = 7.7 Hz, 2H), 7.54 (d, *J* = 7.3 Hz, 2H), 6.75 (d, *J* = 6.6 Hz,

4H), 3.40 (t,  $J = 7.3$  Hz, 8H), 1.57–1.63 (m, 8H), 1.37–1.43 (m, 8H), 0.99 (t,  $J = 7.2$  Hz, 12H). HRMS: calcd for  $C_{42}H_{50}N_6O_2$  [M + H]<sup>+</sup> 671.3995, found 671.4068.

**Synthesis of 1,5-Bis((4-(dimethylamino)phenyl)diazenyl)-anthracene-9,10-dione (Azo-03).** The compound was prepared by treatment of 1,5-diamineanthraquinone (2.48 g, 10 mmol) with *N,N*-dimethylaniline (2.42 g, 20 mmol) as described for **Azo-01**. Yield: 76.40%. <sup>1</sup>H NMR (400 MHz, CDCl<sub>3</sub>)  $\delta$  (ppm): 8.30 (d,  $J = 7.1$  Hz, 2H), 7.90 (d,  $J = 9.5$  Hz, 4H), 7.77 (t,  $J = 9.3$  Hz, 2H), 7.54 (d,  $J = 7.2$  Hz, 2H), 6.75 (d,  $J = 8.2$  Hz, 4H), 3.35 (t,  $J = 7.3$  Hz, 12H). HRMS: calcd for  $C_{42}H_{26}N_6O_2$  [M + H]<sup>+</sup> 503.2117, found 503.2189.

**Synthesis of 4,4'-(1,1'-Biphenyl)-4,4'-diylbis(diazene-2,1-diyl))bis(*N,N*-dibutylaniline) (DIAzo).** The compound was prepared by treatment of benzidine (1.84 g, 10 mmol) with *N,N*-dibutylaniline (4.10 g, 20 mmol) as described for **Azo-01**. Yield: 82.65%. <sup>1</sup>H NMR (400 MHz, CDCl<sub>3</sub>)  $\delta$  (ppm): 7.85 (d,  $J = 8.0$  Hz, 8H), 7.77 (d,  $J = 8.2$  Hz, 4H), 6.72 (d,  $J = 8.2$  Hz, 4H), 3.38 (t,  $J = 7.4$  Hz, 8H), 1.59–1.65 (m, 8 H), 1.33–1.41 (m, 8H), 0.98 (t,  $J = 7.2$  Hz, 12H). HRMS: calcd for  $C_{40}H_{52}N_6$  [M + H]<sup>+</sup> 617.4253, found 617.4971.

**2.3. Fabrication of the Memory Device.** The ITO glass substrates were precleaned in ultrasonic bath for 30 min each in deionized water, acetone, and ethanol. The electroactive organic layer was deposited under a pressure of around  $1.0 \times 10^{-6}$  Torr. The thickness of electroactive organic layer was 85 nm. The 120 nm-thick aluminum (Al) electrodes ( $0.0314 \text{ mm}^2$ ) were vacuum-deposited at  $5.0 \times 10^{-6}$  Torr through a shadow mask to form top electrodes. The device with the structure of ITO/organic compound/Al was obtained.

**2.4. Measurement.** <sup>1</sup>H NMR spectra were obtained on Inova 300 and 400 MHz FT-NMR spectrometers. Thermogravimetric analysis (TGA) was conducted on a TA Instruments Dynamic TGA 2950 at a heating rate of  $10 \text{ }^\circ\text{C min}^{-1}$  and under an N<sub>2</sub> flow rate of  $50 \text{ mL min}^{-1}$ . UV-vis absorption spectra were carried out in the 300–800 nm spectral regions with a Perkin-Elmer Lambda spectrophotometer. Cyclic voltammetry was performed at room temperature using an ITO working electrode, a reference electrode Ag/AgCl, and a counter electrode (Pt wire) at a sweep rate of  $100 \text{ mV s}^{-1}$  on a CorrTest CS Electrochemical Workstation analyzer. A 0.1 M solution of tetrabutylammonium perchlorate (TBAP) in anhydrous acetonitrile was used. SEM images were taken on a Hitachi S-4700 scanning electron microscope. The surface morphology of films was measured on a MFD-3D-SA Asylum Research's atomic force microscope (AFM). X-ray diffraction (XRD) patterns were taken on an X'Pert-Pro MPD X-ray diffractometer. All electrical measurements of the devices were characterized under ambient conditions without any encapsulation using an Agilent Technologies B1500A Semiconductor device Analyzer.

### 3. RESULTS AND DISCUSSION

**3.1. Thermal Properties.** Thermal properties of **Azo-01**, **Azo-02**, and **Azo-03** were investigated by TGA (Figure S1, Supporting Information). All of the compounds exhibit good thermal stability with thermal decomposition temperatures (5% weight loss temperature) of 286 °C (**Azo-01**), 225 °C (**Azo-02**), and 236 °C (**Azo-03**), respectively. It indicates that the materials can endure heat deterioration in the memory devices.<sup>10b</sup>

**3.2. Photophysical and Electrochemical Properties.** Figure 1 shows the UV-vis absorption spectra of **Azo-02** in

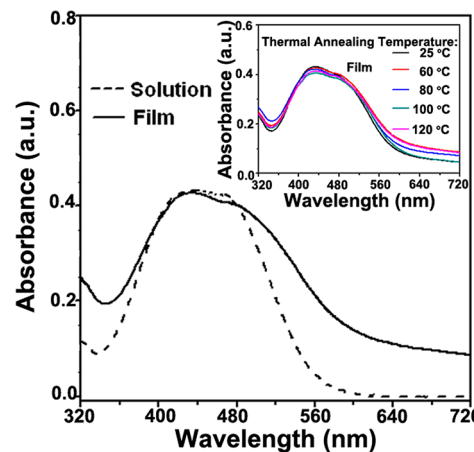


**Figure 1.** UV-vis absorption spectra of **Azo-02** in tetrahydrofuran solution and film states with different thermal annealing temperatures.

anhydrous tetrahydrofuran solution and as thin film deposited on ITO glass substrates. Because of the coupling between the n-π\* and π-π\* transitions of the azobenzene chromophore, the optical absorption spectra of the solution sample show the moderate broad absorption band in the range of 360–480 nm.<sup>32</sup> As compared to the absorption spectra of the solution state, the absorption peaks of **Azo-02** in the film state are significantly broadened. The changes are associated with the formation of molecular aggregation or orderly π-π stacking in the film.<sup>33,34</sup> No significant change in the absorption of **Azo-02** film was observed as the annealing temperature increased, which may contribute to the stability of the device's performance. The absorption peaks of "counterpart" molecule **Azo-01** and **Azo-03** in the film states change slightly as the annealing temperature increased (Figure S2, Supporting Information). The band gap of **Azo-02** between the highest occupied molecular orbital (HOMO) and the lowest unoccupied molecular orbital (LUMO) energy levels estimated from the onset of the absorption spectra is 2.28 eV by the following equation:  $E_g = hc/\lambda_{\text{Edge}}$ .<sup>32</sup> The electrochemical property of **Azo-02** was measured by cyclic voltammetry (CV), as shown in Figure 2. The onset oxidation  $E_{\text{ox}}^{(\text{onset})}$  of **Azo-02** is 0.45 V. Note that the  $E_{\text{Ferrocene}}$  was 0.14 eV from the CV measurement. The HOMO and LUMO energy levels are calculated by the following equation:<sup>32</sup>

$$E_{\text{HOMO}} = -[E_{\text{ox}}^{(\text{onset})} + 4.8 - E_{\text{Ferrocene}}]$$

$$E_{\text{LUMO}} = E_{\text{HOMO}} + E_g$$

where  $E_{\text{HOMO}}$  and  $E_{\text{LUMO}}$  are the HOMO and the LUMO energy levels, and  $E_{\text{ox}}^{(\text{onset})}$  is the onset oxidation potential of the molecule. The HOMO level of **Azo-02** is  $-5.11$  eV, and the LUMO level is  $-2.83$  eV. The energy barrier between Φ of ITO ( $-4.80$  eV) and the HOMO level is  $0.31$  eV, which is much lower than the energy barrier between Φ of Al ( $-4.28$  eV) and LUMO level ( $1.45$  eV). It indicates that the hole injection from ITO into the HOMO of **Azo-02** is much easier than the electron injection from Al into the LUMO level of **Azo-02**. Therefore, **Azo-02** is a p-type material, and holes predominate the conduction process of the memory devices. The "counterpart" molecules **Azo-01** and **Azo-03** are also p-type materials deduced from UV-vis absorption spectra and the CV measurements (Figure 2 and Figure S2a,b of the Supporting Information).<sup>20</sup>

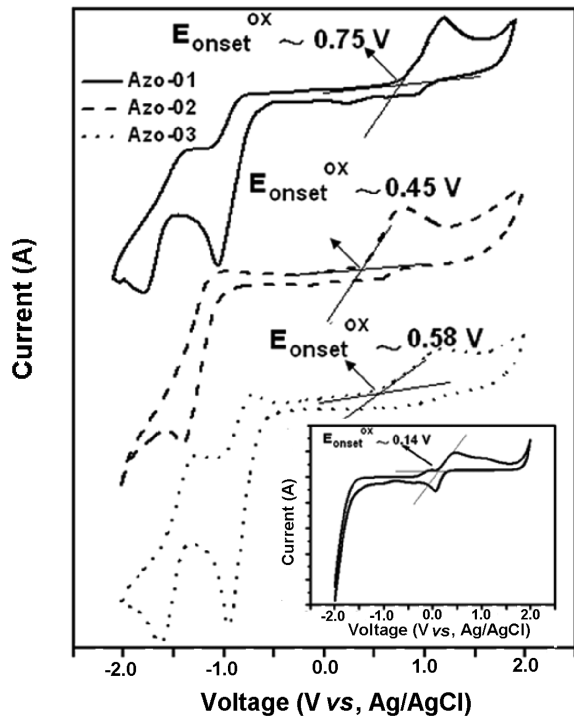


**Figure 2.** Cyclic voltammogram of Azo-01, Azo-02, and Azo-03 in acetonitrile solution with 0.1 M tetrabutylammonium perchlorate as electrolyte and ITO glass as the working electrode. The scanning rate was  $100 \text{ mV s}^{-1}$ .

**3.3. Morphology of Films and Molecular Packing.** The effect of annealing temperature on the superficial morphology can be directly imaged by atomic force microscopy (AFM). Figure 3 shows the tapping-mode AFM height images of 85 nm-thick Azo-02 films vacuum-deposited on the ITO glass substrate at different thermal annealing temperatures for 8 h.

The root-mean-square (rms) values of Azo-02 films are 4.38 nm ( $25^\circ\text{C}$ ), 2.59 nm ( $60^\circ\text{C}$ ), 1.37 nm ( $80^\circ\text{C}$ ), 1.02 nm ( $100^\circ\text{C}$ ), and 0.99 nm ( $120^\circ\text{C}$ ). The smooth morphology of the film facilitates the charge injection from the electrode into the organic molecules.<sup>18a,35</sup> Furthermore, it can prevent the aluminum (Al) electrode happening penetration into the film during the vacuum deposition process.<sup>18b</sup> The rms surface roughness of Azo-01 increases rapidly as annealing temperature increased, as shown in Figure 3f. The AFM images show the formation of molecular aggregation, and numerous film defects appear as the thermal annealing temperature increased (Figure S3a–c, Supporting Information). The rms surface roughness of Azo-03 is the largest and reaches 9 times the thickness of the films at all annealing temperatures (Figure 3f and Figure S3d of the Supporting Information). The above facts indicate that the increase of molecular conjugation and the introduction of flexible alkyl chains are helpful to improve the thermal stability, the smoothness, and the continuity of the films for twisted molecules.

The XRD patterns of Azo-02 films deposited on ITO glass substrate at different annealing temperatures for 8 h are shown in Figure 4. The obvious diffraction peaks are at  $2\theta = 10.61^\circ$  ( $8.33 \text{ \AA}$ ),  $2\theta = 14.97^\circ$  ( $5.91 \text{ \AA}$ ), and  $2\theta = 21.27^\circ$  ( $4.17 \text{ \AA}$ ), indicating the formation of orderly and close crystal.<sup>36,37</sup> Furthermore, the  $2\theta = 10.61^\circ$  ( $8.33 \text{ \AA}$ ) is almost twice that of  $2\theta = 21.27^\circ$  ( $4.17 \text{ \AA}$ ), which indicates the Azo-02 molecule had good layer by layer stacking in the film. This is because the alkyl chains serve as a spacer to control the distance of conjugated backbones and can enhance the intermolecular interactions.<sup>38</sup> The intensity of diffraction peaks does not change significantly as the annealing temperature increases. It indicates the low sensitivity of molecular packing to temperature fluctuation. However, for the films of “counterpart” molecules Azo-01, the intensity of diffraction peaks decreases gradually as the annealing temperature increased (Figure S4a, Supporting

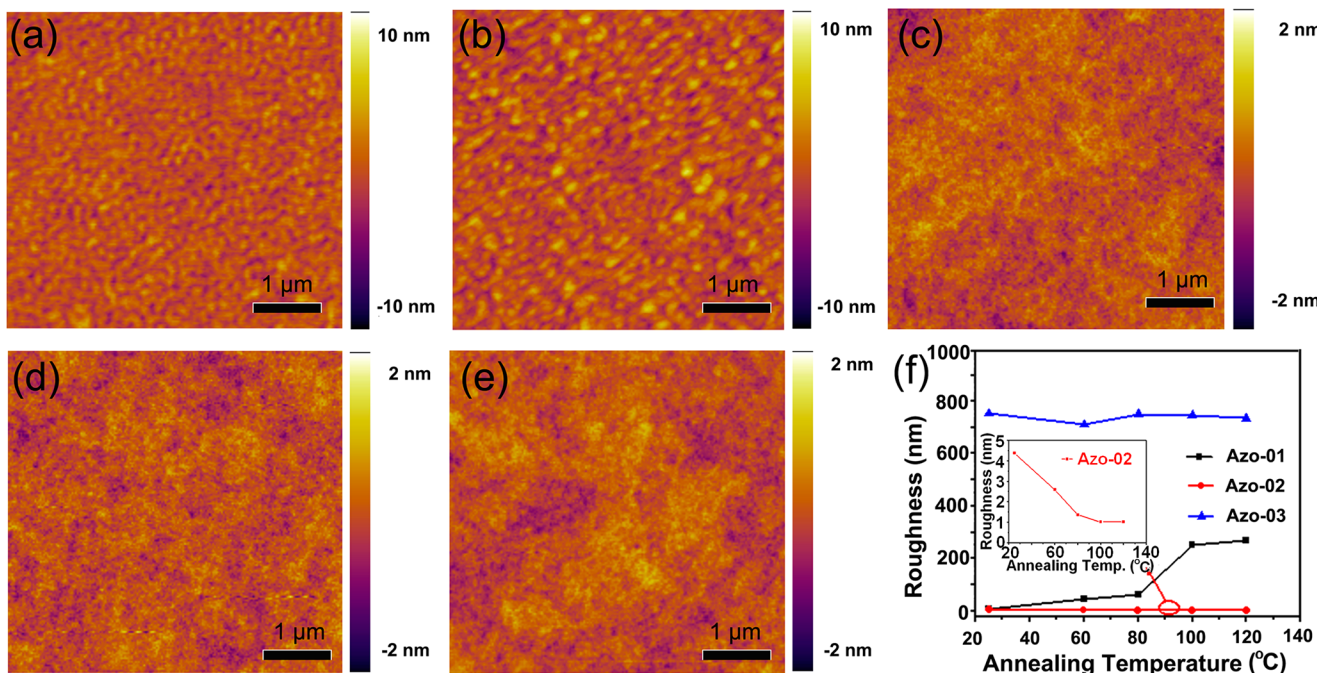


**Figure 3.** The tapping-mode AFM height images of 85 nm-thick Azo-02 films deposited onto ITO glass substrate at (a)  $25^\circ\text{C}$ ; (b)  $60^\circ\text{C}$ ; (c)  $80^\circ\text{C}$ ; (d)  $100^\circ\text{C}$ ; and (e)  $120^\circ\text{C}$  for 8 h. (f) Roughness of films at different thermal annealing temperatures. Each image is  $5 \times 5 \mu\text{m}^2$ .

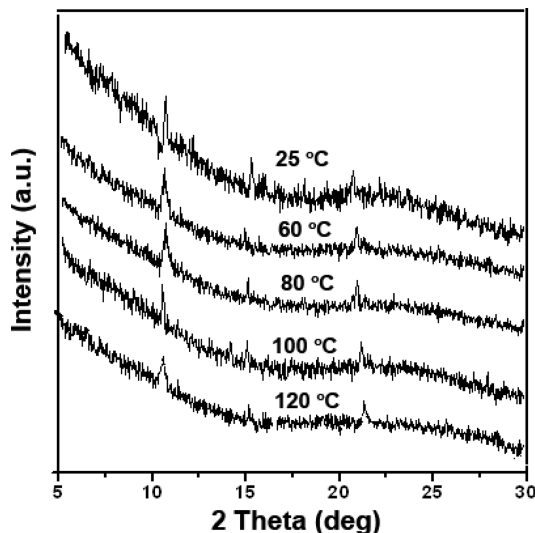


**Figure 4.** X-ray diffraction of 85 nm-thick Azo-02 films deposited on ITO glass substrates at 25, 60, 80, 100, and 120 °C for 8 h.

Information). The results indicate that molecular packing changes obviously as temperature fluctuates. Therefore, the morphology of the film changes significantly. For “counterpart” molecules Azo-03, no discernible XRD peaks are observed for films, indicating a disordered packing (Figure S4b, Supporting Information). The results reflect weaker intermolecular  $\pi$ – $\pi$  stacking interactions.

**3.4. Electrical Switching Effects and Memory Performance.** Memory devices of ITO/Azo/Al sandwich structure were fabricated. The device’s structure and the cross-section view of one storage cell are shown schematically in Figure 5a. The thickness of the electroactive organic layer is about 85 nm, as measured by SEM. Figure 5b shows the current–voltage ( $I$ –

$V$ ) characteristics of the organic memory device, with Azo-02 film annealed at 25 °C as the electroactive layer. When a voltage sweep was applied from 0 to  $-6$  V (with Al as cathode and ITO as anode), the device was initially in the low-conductivity (“0” signal or OFF) state, switched to the intermediate-conductivity (“1” signal or ON1) state at  $-1.35$  V, and then switched to the high-conductivity (“2” signal or ON2) state at  $-2.72$  V. The ON1/OFF and ON2/ON1 current ratios were up to  $2.72 \times 10^3$  and  $1.15 \times 10^2$ . The high current ratios lead to a low misreading rate for memory applications.<sup>39</sup> The ON2 state could not be returned to OFF or ON1 states by subsequent application of a positive sweep from 0 to 6 V, and the device remained in the ON2 state even after the power had been turned off for 10 h. It exhibited typical nonvolatile WORM (write-once-read-many-times) memory behavior. Under a constant stress of  $-1$  V, no obvious degradation in the current was observed for OFF, ON1, and ON2 states over  $10^4$  s, as shown in Figure 5c. In addition, the OFF, ON1, and ON2 states were also stable up to  $10^8$  read pulses of  $-1$  V, as shown in Figure 5d. The switching threshold voltages are all lower than  $-4$  V, and the reading voltage is only  $-1$  V, which indicate that the organic ternary memory device has low power consumption and can be a good supplementary device to the conventional data-storage technology. The  $I$ – $V$  characteristics of the “counterpart” molecules Azo-01 and Azo-03 were also measured under the same conditions. Azo-01 annealed at 25 °C as electroactive layer also exhibited the ternary nonvolatile WORM memory behavior. Its first and second switching threshold voltages were  $-1.43$  and  $-2.81$  V, respectively. The ON1/OFF and ON2/ON1 current ratios were up to  $2.41 \times 10^3$  and  $1.78 \times 10^2$  (Figure S5a, Supporting Information). No abrupt current change for Azo-03 device was observed when the voltage sweep changed from 0 to  $-6$  V, which can be ascribed to the disordered molecular packing (Figure S7, Supporting Information).

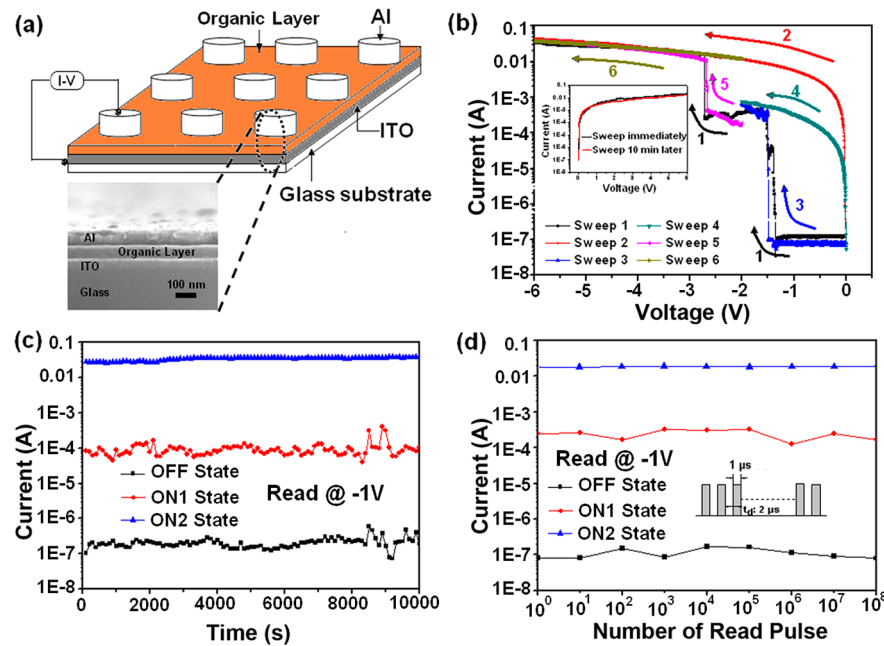


**Figure 5.** (a) Schematic diagram of the device consisting of organic layer sandwiched between an ITO bottom electrode and an Al top electrode; SEM image of one storage cell (cross-section view). (b) Current–voltage ( $I$ – $V$ ) characteristics of the ITO/Azo-02 (25 °C)/Al device. (c) Effect of operation time on the OFF, ON1, and ON2 states of the ITO/Azo-02 (25 °C)/Al device under a constant stress of  $-1$  V. (d) Effect of read pulse of  $-1$  V on the OFF, ON1, and ON2 states of the ITO/Azo-02 (25 °C)/Al device. The inset shows the pulse used for the measurement.

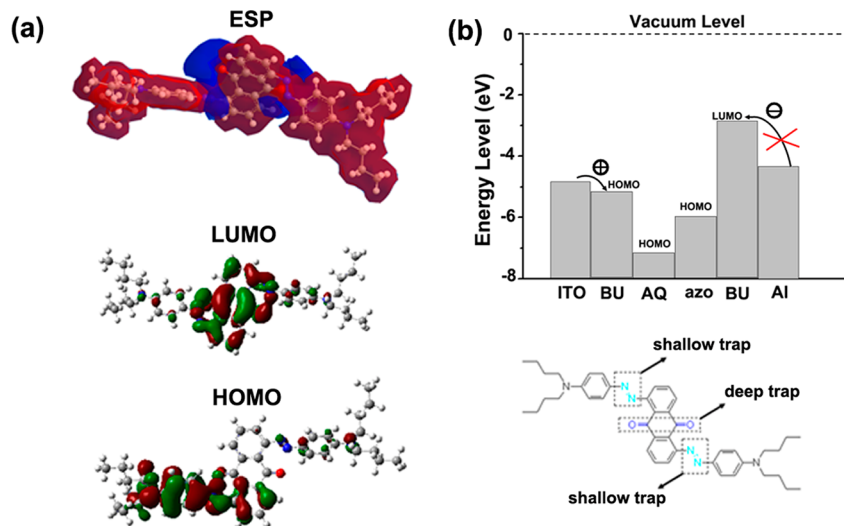


**Figure 6.** DFT molecular simulation results of **Azo-02** at the B3LYP/6-31G(d) level: (a) molecular electrostatic potential (ESP) surfaces and molecular orbitals of the HOMO and LUMO. (b) LUMO and HOMO energy levels for the basic unit (BU: **Azo-02**) and two functional fragments (anthraquinone moiety, AQ; azobenzene chromophore, azo) and the functional groups as the “trap”.

The heat resistance of the devices was also studied. All of the devices fabricated with **Azo-01**, **Azo-02**, and **Azo-03** were prepared under annealing temperatures ranging from 60 to 120 °C. The *I*–*V* curves of the device fabricated with **Azo-01** as the electroactive layer showed the device to be always in a single high-conductivity state, and no conductance switching behavior was observed (Figure S5b, Supporting Information). This is due to the appearance of defects in the film during the annealing process, which may lead to the top and bottom electrodes contact. The *I*–*V* curves of the device fabricated with **Azo-02** as the electroactive layer showed similar memory behavior as compared to the performance of the device at 25 °C, with basically the same switching threshold voltages and ON/OFF current ratios (Figure S6, Supporting Information). No sharp current changes have been observed on device fabricated with **Azo-03** as the electroactive layer at the different annealing temperatures (Figure S7, Supporting Information). This is further confirmed in that the molecule with the combination of large conjugated backbones and long alkyl chains can enhance the thermal stability of the device.

The electrical and switching characteristics of organic memory devices originating from the formation of metallic filaments have been reported previously.<sup>40</sup> To exclude the roles of metallic filaments or oxide layer ( $\text{Al}_2\text{O}_3$  layer between the Al electrode and organic layer) in the ternary electrical switching, the device was fabricated with **Azo-02** film as the electroactive layer and mercury beads (Hg) of different diameter as the top electrode for two advantages. First, mercury is one of the less reactive metals and is much more stable than Al in the atmosphere of oxygen. Second, Hg is not infiltrated into the film easily to form the metallic filaments. Tristable conductance switching behaviors were also obtained via ITO/**Azo-02**/Hg device (Figure S8, Supporting Information). Devices with different active areas (mercury electrode) show almost the same *I*–*V* characteristics, which indicate that the currents of three conductive states based on **Azo-02** are independent of the active areas. We removed one functional moiety of molecule and fabricated the device ITO/DIAzo/Al at the same condition. The device exhibited electrical bistability with the switching threshold voltage of  $-1.38$  V and ON/OFF current

of  $3.58 \times 10^2$  (Figure S9, Supporting Information). In addition, when we only retained the functional moiety, anthraquinone, the molecule also exhibited a binary memory effect with larger switching threshold and ON/OFF current ratio. It indicated that the ternary effect of the studied molecule was the result of the synergy of the two functional moieties.

**3.5. Proposed Storage Mechanism.** To better understand the switching behavior of the devices, the molecular conformation and electronic properties of **Azo-02** were explored through density functional theory. Figure 6a shows the molecular surfaces with the continuous electrostatic potentials (ESP) in the red area. It indicates that charges can migrate through this open channel.<sup>10b</sup> However, there are some negative ESP regions (blue), which arise from the azobenzene chromophore and anthraquinone moiety. These negative regions can serve as a “trap” to localize the charge, leading to charge retention and memory effects.<sup>9a</sup> The depth of these traps is in accordance with the electron-withdrawing ability of the functional groups, and the depth values of each trap were simulated by reference to the reported methods in the literature.<sup>41</sup> The energy levels of the HOMO and LUMO for basic unit (BU: **Azo-02**) and functional fragments (anthraquinone moiety, AQ; azobenzene chromophore, azo) are shown in Figure 6b and Figure S10 of the Supporting Information. The trap depth aroused from azobenzene chromophore moiety is about 1.16 eV, while that aroused from anthraquinone moiety is about 2.30 eV (Figure 6b). Therefore, the former is a shallower trap, and the latter is the deeper one. Because of the orderly and close molecular packing, charges transfer among the adjacent molecules easily, and all of the traps have equal opportunities to accept the injected charges. When the shallower traps arising from the azobenzene chromophore are filled completely, the storage cell switches from OFF state to ON1 state. When the second switching threshold voltage comes, the deeper traps arising from the anthraquinone moiety are filled, and the storage cell switches from ON1 state to ON2 state. Figure 6a shows that the electron was located on the electron donor side totally transit to the electron acceptor side to form an obvious charge-separated state upon the HOMO to LUMO transition. The trapped electrons are hard to detract by

the reverse electric field, and the obvious charge-separated state will not revert to the pristine state and the high-conductivity can be maintained for a long time. Therefore, the device exhibits WORM behavior.

#### 4. CONCLUSIONS

Three conjugated and twisted anthraquinone azo compounds were synthesized and demonstrated the effects of conjugated structure and long flexible chains. The devices based on a molecule with the combination of large conjugated backbones and long alkyl chains exhibited stable nonvolatile ternary memory behavior as the thermal annealing temperature increased. The switching threshold voltages and ON/OFF current ratios are basically the same. It is due to the low sensitivity of molecular packing to temperature fluctuation and the formation of more ordered and closer packed crystalline film. The “counterpart” molecule (with shorter conjugated backbones or shorter alkyl chains) film has defects and disordered crystal packing, and even no obvious conductance switching behaviors were observed for the corresponding memory devices. The large conjugated backbones and longer alkyl chains are believed to play vital roles in the electroactive layer and the device’s performance by enhancing the intermolecular interactions. We hope these results can provide a reference to the design of future ultrahigh density storage materials and stable memory device.

#### ■ ASSOCIATED CONTENT

##### Supporting Information

Figures S1–S10. This material is available free of charge via the Internet at <http://pubs.acs.org>.

#### ■ AUTHOR INFORMATION

##### Corresponding Author

\*E-mail: liujm@suda.edu.cn (J.L.); lihuaw@suda.edu.cn (H.L.).

##### Notes

The authors declare no competing financial interest.

#### ■ ACKNOWLEDGMENTS

This work was financially supported by the Chinese Natural Science Foundation (21076134, 21176164, and 21206102), NSF of Jiangsu Province (BK2010208), a project of Jiangsu Education Department (12KJB430011), Suzhou Nanoproject (ZXG2012023), a project supported by the Specialized Research Fund for the Doctoral Program of Higher Education of China (Grant No. 20113201130003), and a project funded by the Priority Academic Program Development of Jiangsu Higher Education Institutions (PAPD).

#### ■ REFERENCES

- (1) Lee, J.; Lee, E.; Kim, S.; Bang, G. S.; Shultz, D. A.; Schmidt, R. D.; Forbes, M. D. E.; Lee, H. *Angew. Chem., Int. Ed.* **2011**, *50*, 4414–4418.
- (2) Lee, J. S. *J. Mater. Chem.* **2011**, *21*, 14097–14112.
- (3) Scott, J. C.; Bozano, L. D. *Adv. Mater.* **2007**, *19*, 1452–1463.
- (4) You, N. H.; Chueh, C. C.; Liu, C. L.; Ueda, M.; Chen, W. C. *Macromolecules* **2009**, *42*, 4456–4463.
- (5) Son, D. I.; Kim, T. W.; Shim, J. H.; Jung, J. H.; Lee, D. U.; Lee, J. M.; Park, W. I.; Choi, W. K. *Nano Lett.* **2010**, *10*, 2441–2447.
- (6) Chu, C. W.; Ouyang, J.; Tseng, J. H.; Yang, Y. *Adv. Mater.* **2005**, *17*, 1440–1443.
- (7) Ling, Q. D.; Liaw, D. J.; Zhu, C.; Chan, D. S. H.; Kang, E. T.; Neoh, K. G. *Prog. Polym. Sci.* **2008**, *33*, 917–978.
- (8) (a) Ling, Q. D.; Chang, F. C.; Song, Y.; Zhu, C. X.; Liaw, D. J.; Chan, D. S. H.; Kang, E. T.; Neoh, K. G. *J. Am. Chem. Soc.* **2006**, *128*, 8732–8733. (b) Kim, D. M.; Park, S.; Lee, T. J.; Hahm, S. G.; Kim, K.; Kim, J. C.; Kwon, W.; Ree, M. *Langmuir* **2009**, *25*, 11713–11719. (c) Kuorosawa, T.; Chueh, C. C.; Liu, C. L.; Higashihara, T.; Ueda, M.; Chen, W. C. *Macromolecules* **2010**, *43*, 1236–1244. (d) Liu, S. J.; Lin, Z. H.; Zhao, Q.; Ma, Y.; Shi, H. F.; Yi, M. D.; Ling, Q. D.; Fan, Q. L.; Zhu, C. X.; Kang, E. T.; et al. *Adv. Funct. Mater.* **2011**, *21*, 979–985. (e) Hahm, S. G.; Choi, S.; Hong, S. H.; Lee, T. J.; Park, S.; Kim, D. M.; Kwon, W. S.; Kim, K.; Kim, O.; Ree, M. *Adv. Funct. Mater.* **2008**, *18*, 3276–3282. (f) Zhuang, X. D.; Chen, Y.; Li, B. X.; Ma, D. G.; Zhang, B.; Li, Y. *Chem. Mater.* **2010**, *22*, 4455–4461. (g) Kim, K.; Park, S.; Hahm, S. G.; Lee, T. J.; Kim, D. M.; Kim, J. C.; Kwon, W.; Ko, Y. G.; Ree, M. *J. Phys. Chem. B* **2009**, *113*, 9143–9150.
- (9) (a) Lee, W. Y.; Kurosawa, T.; Lin, S. T.; Higashihara, T.; Ueda, M.; Chen, W. C. *Chem. Mater.* **2011**, *23*, 4487–4497. (b) Ma, Y.; Cao, X.; Li, G.; Wen, Y.; Yang, Y.; Wang, J.; Du, S.; Yang, L.; Gao, H.; Song, Y. *Adv. Funct. Mater.* **2010**, *20*, 803–810. (c) Shang, Y.; Wen, Y.; Li, S.; Du, S.; He, X.; Cai, L.; Li, Y.; Yang, L.; Gao, H.; Song, Y. *J. Am. Chem. Soc.* **2007**, *129*, 11674–11675.
- (10) (a) Lim, S. L.; Li, N. J.; Lu, J. M.; Ling, Q. D.; Zhu, C. X.; Kang, E. T.; Neoh, K. G. *ACS Appl. Mater. Interfaces* **2009**, *1*, 60–71. (b) Li, H.; Li, N. J.; Sun, R.; Gu, H. W.; Ge, J. F.; Lu, J. M.; Xu, Q. F.; Xia, X. W.; Wang, L. H. *J. Phys. Chem. C* **2011**, *115*, 8288–8294. (c) Fang, Y. K.; Liu, C. L.; Chen, W. C. *J. Mater. Chem.* **2011**, *21*, 4778–4786.
- (11) (a) Lim, S. L.; Ling, Q.; Teo, E. Y. H.; Zhu, C. X.; Chan, D. S. H.; Kang, E. T.; Neoh, K. G. *Chem. Mater.* **2007**, *19*, 5148–5157. (b) Xie, L. H.; Ling, Q. D.; Hou, X. Y.; Huang, W. *J. Am. Chem. Soc.* **2008**, *130*, 2120–2121.
- (12) Yang, Y.; Ouyang, J.; Ma, L.; Tseng, R. J. H.; Chu, C. W. *Adv. Funct. Mater.* **2006**, *16*, 1001–1014.
- (13) Liu, S. J.; Wang, P.; Zhao, Q.; Yang, H. Y.; Wong, J.; Sun, H. B.; Dong, X. C.; Lin, W. P.; Huang, W. *Adv. Mater.* **2012**, *24*, 2901–2905.
- (14) Jung, Y.; Lee, S. H.; Jennings, A. T.; Agarwal, R. *Nano Lett.* **2008**, *8*, 2056–2062.
- (15) Li, H.; Xu, Q. F.; Li, N. J.; Sun, R.; Ge, J. F.; Lu, J. M.; Gu, H. W.; Yan, F. *J. Am. Chem. Soc.* **2010**, *132*, 5542–5543.
- (16) Griffini, G.; Douglas, J. D.; Piliego, C.; Holcombe, T. W.; Turri, S.; Fréchet, J. M. J.; Mynar, J. L. *Adv. Mater.* **2011**, *23*, 1660–1664.
- (17) Jorgensen, M.; Norrman, K.; Krebs, F. C. *Sol. Energy Mater. Sol. Cells* **2008**, *92*, 686–714.
- (18) (a) Zhuang, X. D.; Chen, Y.; Liu, G.; Zhang, B.; Neoh, K. G.; Kang, E. T.; Zhu, C. X.; Li, Y. X.; Niu, L. J. *Adv. Funct. Mater.* **2010**, *20*, 2916–2922. (b) Liu, C. L.; Hsu, J. C.; Chen, W. C.; Sugiyama, K.; Hirao, A. *ACS Appl. Mater. Interfaces* **2009**, *9*, 1974–1979.
- (19) (a) Lee, J. K.; Ma, W. L.; Brabec, C. J.; Yuen, J.; Moon, J. S.; Kim, J. Y.; Lee, K.; Bazan, G. C.; Heeger, A. J. *J. Am. Chem. Soc.* **2008**, *130*, 3619–3623. (b) Verploegen, E.; Mondal, R.; Bettinger, C. J.; Sok, S.; Toney, M. F.; Bao, Z. *Adv. Funct. Mater.* **2010**, *20*, 3519–3529.
- (20) Li, H.; Li, N. J.; Gu, H. W.; Xu, Q. F.; Yan, F.; Lu, J. M.; Xia, X. W.; Ge, J. F.; Wang, L. H. *J. Phys. Chem. C* **2010**, *114*, 6117–6122.
- (21) Tang, M. L.; Roberts, M. E.; Locklin, J. J.; Ling, M. M.; Meng, H.; Bao, Z. *Chem. Mater.* **2006**, *18*, 6250–6257.
- (22) (a) Conings, B.; Bertho, S.; Vandewal, K.; Senes, A.; Haen, J. D.; Manca, J.; Janssen, R. A. J. *Appl. Phys. Lett.* **2010**, *96*, 163301–163303. (b) Yang, X. N.; Loos, J.; Veenstra, S. C.; Verhees, W. J. H.; Wienk, M. M.; Kroon, J. M.; Michels, M. A. J.; Janssen, R. A. J. *Nano Lett.* **2005**, *5*, 579–583. (c) Yang, X. N.; Duren, J. K. J. v.; Janssen, R. A. J.; Michels, M. A. J.; Loos, J. *Macromolecules* **2004**, *37*, 2151–2158. (d) Sivila, K.; Luscombe, C. K.; Thompson, B. C.; Fréchet, J. M. J. *J. Am. Chem. Soc.* **2006**, *128*, 13988–13989.
- (23) (a) Drees, M.; Hoppe, H.; Winder, C.; Neugebauer, H.; Sariciftci, N. S.; Schwinger, W.; Schaffler, F.; Topf, C.; Scharber, M. C.; Zhu, Z. G.; et al. *J. Mater. Chem.* **2005**, *15*, 5158–5163. (b) Miyamoto, S.; Tajima, K.; Hashimoto, K. *Macromolecules* **2009**, *42*, 1610–1618.
- (24) Kim, B. J.; Miyamoto, Y.; Ma, B.; Fréchet, J. M. J. *Adv. Funct. Mater.* **2009**, *19*, 2273–2281.
- (25) Jang, J.; Nam, S.; Chung, D. S.; Kim, S. H.; Yun, W. M.; Park, C. E. *Adv. Funct. Mater.* **2010**, *20*, 2611–2618.

- (26) Sun, Y.; Ma, Y.; Liu, Y.; Lin, Y.; Wang, Z.; Wang, Y.; Di, C.; Xiao, K.; Chen, X.; Qiu, W.; et al. *Adv. Funct. Mater.* **2006**, *16*, 426–432.
- (27) Thiebaut, O.; Bock, H.; Grelet, E. *J. Am. Chem. Soc.* **2010**, *132*, 6886–6887.
- (28) Miao, S. F.; Li, H.; Xu, Q. F.; Li, N. J.; Zheng, J. W.; Sun, R.; Lu, J. M.; Li, C. M. *J. Mater. Chem.* **2012**, *22*, 16582–16589.
- (29) Viswanathan, N. K.; Kim, D. Y.; Bian, S. P.; Williams, J.; Liu, W.; Li, L.; Samuelson, L.; Kumar, J.; Tripathy, S. K. *J. Mater. Chem.* **1999**, *9*, 1941–1955.
- (30) Latef, A.; Bernede, J. C. *Thin Solid Films* **1991**, *204*, 9–12.
- (31) Mahajan, A.; Bedi, R. K.; Kumar, P. S. *Thin Solid Films* **2001**, *398*, 82–86.
- (32) Liu, G.; Zhang, B.; Chen, Y.; Zhu, C. X.; Zeng, L.; Chan, D. S.; Neoh, K. G.; Chen, J.; Kang, E. T. *J. Mater. Chem.* **2011**, *21*, 6027–6033.
- (33) Surin, M.; Sonar, P.; Grimsdale, A. C.; Müllen, K.; Feyter, S. D.; Habuchi, S.; Sarzi, S.; Braeken, E.; Heyen, A. V.; Auweraer, M. V. d.; et al. *J. Mater. Chem.* **2007**, *17*, 728–735.
- (34) Schmidt, R.; Oh, J. H.; Sun, Y. S.; Deppisch, M.; Krause, A. M.; Radacki, K.; Braunschweig, H.; Könemann, M.; Erk, P.; Bao, Z.; et al. *J. Am. Chem. Soc.* **2009**, *131*, 6215–6228.
- (35) Ma, W.; Yang, G.; Gong, X.; Lee, K.; Heeger, A. J. *Adv. Funct. Mater.* **2005**, *15*, 1617–1622.
- (36) Coropceanu, V.; Cornil, J.; Filho, D. A. d. S.; Olivier, Y.; Silbey, R.; Brédas, J. L. *Chem. Rev.* **2007**, *107*, 926–952.
- (37) Katz, H. E.; Lovinger, A. J.; Johnson, J.; Kloc, C.; Siegrist, T.; Li, W.; Lin, Y. Y.; Dodabalapur, A. *Nature* **2000**, *478*–481.
- (38) Mei, J.; Kim, D. H.; Ayzner, A. L.; Toney, M. F.; Bao, Z. *J. Am. Chem. Soc.* **2011**, *133*, 20130–20133.
- (39) Liu, C. L.; Kurosawa, T.; Yu, A. -D.; Higashihara, T.; Ueda, M.; Chen, W. C. *J. Phys. Chem. C* **2011**, *115*, 5930–5939.
- (40) (a) Kwan, W. L.; Lei, B.; Shao, Y.; Prikhodko, S. V.; Bodzin, N.; Yang, Y. *J. Appl. Phys.* **2009**, *105*, 124516–124520. (b) Lei, B.; Kwan, W. L.; Shao, Y.; Yang, Y. *Org. Electron.* **2009**, *10*, 1048–1053. (c) Verbakel, F.; Meskers, S. C. J.; Janssen, R. A. J.; Gomes, H. L.; Cölle, M.; Büchel, M.; Leeuw, D. M. d. *Appl. Phys. Lett.* **2007**, *91*, 192101–192103. (d) Cölle, M.; Büchel, M.; Leeuw, D. M. d. *Org. Electron.* **2006**, *7*, 305–312.
- (41) Ling, Q. D.; Song, Y.; Lim, S. L.; Teo, E. Y. H.; Tan, Y. P.; Zhu, C.; Chan, D. S. H.; Kwong, D. L.; Kang, E. T.; Neoh, K. G. *Angew. Chem., Int. Ed.* **2006**, *45*, 2947–2951.